



doi:10.1016/S0016-7037(00)00449-6

Experimental partitioning of Tc, Mo, Ru, and Re between solid and liquid during crystallization in Fe-Ni-S

C. LAZAR,¹ D. WALKER,^{1,*} and R. J. WALKER²¹Lamont-Doherty Earth Observatory and Department of Earth and Environmental Sciences, Columbia University, Palisades, NY 10964, USA²Department of Geology, University of Maryland, College Park, MD 20742, USA

(Received January 28, 2003; accepted in revised form June 24, 2003)

Abstract—Technetium isotopes ⁹⁷Tc, ⁹⁸Tc and ⁹⁹Tc decay to ⁹⁷Mo, ⁹⁸Ru and ⁹⁹Ru, with half-lives of 2.6 My, 4.1 My, and 0.21 My respectively. If there were early solar system processes that resulted in significant fractionation of Tc from the daughter elements, decay of extant Tc could have led to the creation of Mo and Ru isotopic heterogeneities. To assess the potential of metallic core crystallization to fractionate these elements, we examine the partitioning behavior of Tc relative to Re, Mo and Ru in the Fe-Ni-S system between solid metal and liquid metal alloy. The experimental evidence shows that Tc behaves more like the modestly compatible siderophile element Ru than the more highly compatible siderophile element Re, and that Tc is substantially more compatible than Mo. We also demonstrate a pressure effect in the partitioning of Mo during the crystallization of Fe-Ni-S melts. For a sulfur concentration in the liquid fraction of the core of 10 wt% (16.3 at%), the Jones and Malvin (1990) parameter is $-\ln(1-2 \times 1.09 \times 0.163) \cong 0.44$, which yields: $D(\text{Re}) \cong 4.1$; $D(\text{Ru}) \cong 2.3$; $D(\text{Tc}) \cong 1.7$; $D(\text{Mo})_{\text{Lo-P}} \cong 1.0$; and $D(\text{Mo})_{\text{Hi-P}} \cong 0.5$. Our results suggest that detectable Tc-induced isotopic anomalies ($\geq 0.1 \epsilon$ unit) in Ru and Mo could only be produced by unrealistically extreme degrees of crystallization of metal during asteroidal core fractionation, regardless of the time scales and initial Tc abundances involved. Copyright © 2004 Elsevier Ltd

1. INTRODUCTION

The short-lived ⁹⁷Tc-⁹⁷Mo, ⁹⁸Tc-⁹⁸Ru, and ⁹⁹Tc-⁹⁹Ru isotopic systems are potentially useful as chronometers of early solar system events, and could serve as valuable complements to systems that are based on the decay of other short-lived nuclides, such as ¹⁰⁷Pd-¹⁰⁷Ag, ⁵³Mn-⁵³Cr, and ¹⁸²Hf-¹⁸²W. Compared to these systems, however, the potential Tc-based chronometers are problematic because all isotopes of Tc are relatively short-lived and, therefore, the ratio of Tc to the daughter elements cannot be directly measured. Further, the geochemical behavior of Tc in high temperature systems cannot be empirically constrained. Some recent studies of Mo and Ru isotopes in chondritic and iron meteorites have reported anomalous compositions compared with terrestrial standards (e.g., Yin, 1995; Yin and Jacobsen, 1998; Lu and Masuda, 2000a,b; Dauphas et al., 2002; Yin et al., 2002). Some of these isotopic heterogeneities may be attributable to Tc decay, others may reflect nebular heterogeneities. Indeed there remains a question as to which, if any, isotopic heterogeneities are real. Several other studies of Mo and Ru in bulk irons and chondrites have reported isotopic compositions that are indistinguishable from terrestrial standards (Lu and Masuda, 1994; Becker et al., 2002; Becker and Walker, 2003a,b; Lee and Halliday, 2002). Thus, it remains unknown what level of isotopic heterogeneity is present for Ru and Mo in early solar system materials, and whether any of the putative anomalous compositions are the result of Tc decay. Knowledge of the partitioning behavior of the participant elements will be a major aid in the identification and interpretation of any confirmed anomalous isotopic compositions.

Although there have been some published reports of $D(\text{Mo})$ (Mo concentration in solid metal/Mo concentration in liquid metal sulfide alloy) (Jones and Drake, 1986; Lodders and Palme, 1991; Liu and Fleet, 2000) and $D(\text{Ru})$ (Fleet et al., 1999), no previous study of the partitioning of Tc between solid metal and sulfide liquid has been published, presumably because of the complications associated with obtaining and handling this radioactive element. We present new Tc partitioning data and attempt to reproduce previously published reports of Mo and Ru. We report Re data as a monitor of the compatibility of our experimental technique with previous studies of Re (Jana and Walker, 1997; Fleet et al., 1999; Walker, 2000). Rhenium data also tests the assumption this very highly compatible siderophile element is a reasonable analog for Tc under these conditions (Yin and Jacobsen, 1998; Yin et al., 1999). In the absence of data to the contrary, such analog behavior is expected from the position of Tc above Re in the periodic table.

2. EXPERIMENTAL METHODS

A bulk composition was synthesized to simulate a crystallizing planetary core by mixing elemental Fe-Ni-S powders to respective weight percents of 80–10–10. Although a range of nonmetals may be present in planetary cores, S is an archetypal nonmetal ingredient whose abundance is likely to pass through 10% during core crystallization.

Jones and Malvin (1990) showed that nonmetal abundance was a much more important control on partitioning than temperature. The model of Jones and Malvin is based upon the proposition that tracers either avoid or are attracted to the nonmetals in the liquid. The strength and sign of this interaction is one system parameter, β , the matrix constitution cipher, α , being the other. From these two parameters and the content of the nonmetal in the liquid, the partitioning D can be calculated according to the Jones and Malvin parameterization without knowledge of temperature. The extent to which a system follows this parameterization can be determined by knowing how well behaved are plots like Figures 4 to 6. The slopes of such plots can be used to find

* Author to whom correspondence should be addressed (dwalker@ldeo.columbia.edu).

the β parameter. In a system such as Fe-Ni-S which obeys Jones and Malvin systematics the specific choice of 10% S for an experimental bulk composition is not restrictive because the Jones and Malvin systematics can be used to evaluate any other S content one wishes.

After grinding the Fe-Ni-S powders under alcohol to ensure homogeneity, the mixture was dried in a vacuum furnace and stored in a sealed bottle placed in a desiccator. Technetium was purchased from Oak Ridge National Laboratories (ORNL) as a waste stock of oxidized metal powder stored in air. A 1995 ICP-MS analysis from ORNL reported a weight percent composition of 77.9% Tc (22.1% O assumed by difference). This Tc-oxide was reduced by Ti metal in a vacuum-sealed silica tube at 800°C at the Lamont-Doherty Earth Observatory. In experiments BB-753 to BB-757, Mo was added as a mixture of Mo and MoO₃ (wt, 77.2 Mo/22.8 O) to approximate the ORNL Tc/O ratio and assess the effect of a slightly oxidized tracer in the event of incompletely reduced Tc. For the remaining non-Tc experiments, the siderophile element tracers were added as elemental powders of Mo, Ru, and Re. Starting compositions, run temperatures, and run durations for all experiments are listed in Table 1.

Our experimental methods are essentially identical to those of Walker (2000) and will not be reintroduced in detail here: multi-anvil techniques using inverted temperature gradients in sintered MgO capsules with percent-level dopings of the siderophile elements of interest. Very small weighed aliquots of metal and/or oxide siderophile element tracer(s) were placed on the bottom of an MgO capsule and buried with Fe-Ni-S. The capsule was placed in an 8-mm TEL octahedron lined with a LaCrO₃ heater and penetrated by a W-Re thermocouple. This assembly was then loaded into a multianvil apparatus described in Walker et al. (1990) and Walker (1991). Experimental runs were pressurized to 60 kbar, and heated to 800°C (below the Fe-Ni-S solidus) for at least 8 h to allow the MgO to sinter. The temperature was then raised to the thermal regime of interest (950°C to 1325°C) and left for 6–72 h. The typical yield (Fig. 1, first frame) was a well-segregated layer of Fe-Ni alloy overlying a quenched liquid region of sulfide with microscopic metal dendrites. Multianvil techniques are not necessary a priori. The nonstandard multianvil techniques of Walker (2000) were adopted because of their success in previous studies from this lab where they are routine. They avoid potential difficulties with the persistence of refractory nuggets sometimes encountered in standard low-pressure sealed silica tube experiments as reported by, e.g., Wang (1993) and Fleet et al. (1999). The use of a multianvil strategy was not thought to compromise the relevance of the observations to either low or high-pressure applications because Jones and Walker (1991) and Walker (2000) concluded that pressure was not an important determinant of partitioning behavior in these systems up to at least ~100 kbar. Our discovery of a substantial pressure effect in Mo partitioning, documented below, was therefore an initially unwelcome surprise.

3. ANALYSIS

Experiments BB-724 through BB-747 were analyzed on the Lamont-Doherty CAMECA electron microprobe at a 15 kV gun voltage and a 50 nA sample current. Ruthenium and Re were analyzed using the $L\alpha$ lines and ± 800 spectrometer steps off peak for measuring background corrections. (There are 10⁵ spectrometer steps between Bragg angle $\sin \Theta$ of 0 and 1.) Molybdenum was analyzed using its $L\alpha$ line with a background of +400/–2000 spectrometer steps to avoid interference with the S $K\alpha$. When the Mo results appeared inconsistent with the previous study of Liu and Fleet (2000), we prepared experiments BB-751, BB-758, BB-759, and BB-760 with increased tracer concentrations to improve the counting statistics. These experiments were analyzed at 20–25 kV and 75–100 nA; Mo was analyzed using the $L\beta$ line, which is free of interferences.

Ni ($K\alpha$), Mo ($L\beta$), and Re ($L\alpha$) were standardized with pure, industrially prepared metal. S ($K\alpha$) was standardized with pyrite, Fe ($K\alpha$) with chalcopyrite, O ($K\alpha$) with hematite, and Ru ($L\alpha$) with hot-pressed pure metal powder. A tracer-free Fe-Ni-S charge was used to check background count measure-

ments for the tracers at various voltages and currents. Since a measurable concentration of Ti was present in the Tc experiments, we include Ti data, standardized to $K\alpha$ in pure Ti metal. Atomic fractions, as analyzed and calculated by the probe and its software, were used to calculate $D = (\text{atomic fraction in solid metal}/\text{atomic fraction in liquid metal})$.

The Tc standard was hot-pressed from the reduced Tc metal powder. To determine the Tc concentration of the standard, we plotted the count rates versus atomic number of the $L\alpha$ lines of the pure transition metals that flank Tc in the periodic table. Figure 2 demonstrates that the plot of the pure elements, Zr, Nb, Mo, Ru, Rh, Pd, and Ag, is smoothly varying, allowing an interpolation to approximate the count rate of pure Tc. We used a linear interpolant to calculate a theoretical count rate for pure Tc of 10,700 counts per second (c/s). (A polynomial interpolant gives a number within the fitting error of the linear choice. The D values eventually calculated do not depend on this choice.) The Tc standard yielded 8800 c/s, 82% of the pure count rate. A complete wavelength scan of the standard yielded significant concentrations of Ti, Si, and O. After standardizing for these contaminants, the Tc standard was analyzed with a procedure programmed with the approximated Tc standard, Ti, Si, and O. Several small raster mode analyses spaced throughout a well-polished, optically clean region of the standard, yielded an average weight percent composition of 80% Tc, 15.5% Ti, 3.5% Si, and 1% O (possibly surface contamination). The total weight percents of these test analyses averaged to 100% \pm 2–3%; this result provided an iterative crosscheck on our first Tc approximation.

The sulfide composition was analyzed in small raster mode (at 800 \times magnification, a small raster is a square 30 μm on a side) under the assumption that the spatial averaging of many local dendrite + matrix compositions will statistically recreate the equilibrium composition of the once-homogeneous sulfide. Uncertainties were reported as standard deviations (σ) of the means, calculated by σ/\sqrt{n} , where 'n' is the number of raster analyses, because we are interested in the expected uncertainty of the once-homogeneous sulfide composition, not in the compositional variation from point to point which is an artifact of the phase separation during quenching. The composition of liquid reported in Table 1 is the average of the rasters. The solid metal was analyzed using point mode to maximize spatial resolution at the metal-sulfide interface. This method allowed us to pinpoint the onset of quench-related disruptions in the otherwise continuous, monotonic variation in trace element concentrations approaching the interface with the liquid. The distinct gradients in some of the solid metal ingredients are the result of a complex interplay between liquid-state diffusion feeding the growing solid metal layer, solid-state diffusion erasing those genetic stratigraphic gradients, and thermal migration refinement of the consolidating metal layer as the experiment matures. Details of this complex process are reviewed in Walker (2000). The solid metal compositions given in Table 1 are averages of those at the interface (that most closely reflect solid/liquid equilibration). Figure 3 shows a compositional traverse in experiment BB-730, a micrograph of which appears in the central frame of Figure 1. Within a given charge, we observed minor variations in metal composition along the strike of the metal/sulfide interface, but this did not

Table 1. Experimental partitioning results.^a

Element	Starting comp.		Metal (at frac.)		Liquid (at frac.)		D	±	±
	wt %	At. Frac.	Avg	SD	Avg	$\sigma/\text{sqr}t(n)$	Metal/sulfide		%
BB-724 (9 h, 1325°C)									
Fe	78.47	0.738	0.8772	0.0046	0.7129	0.0021	1.23	0.01	1
Ni	10	0.090	0.1155	0.0048	0.1076	0.0011	1.07	0.06	6
S	10	0.164	0.0029	0.0012	0.1750	0.0030			
Mo	0.77	0.004	0.0017	0.0002	0.0034	0.0000	0.50	0.06	12
Ru	0.77	0.004	0.0026	0.0003	0.0010	0.0000	2.60	0.30	12
BB-728 (19 h, 1210°C)									
Fe	79.08	0.741	0.8637	0.0032	0.6336	0.0016	1.36	0.01	1
Ni	10.08	0.090	0.1253	0.0027	0.1073	0.0016	1.17	0.04	3
S	10.08	0.165	0.0031	0.0002	0.2542	0.0024			
Ru	0.77	0.004	0.0066	0.0002	0.0014	0.0000	4.71	0.15	3
BB-729 (24 h, 1200°C)									
Fe	77.86	0.737	0.8703	0.0008	0.6374	0.0023	1.37	0.00	0
Ni	9.92	0.089	0.0979	0.0002	0.0906	0.0005	1.08	0.01	1
S	9.92	0.164	0.0018	0.0000	0.2633	0.0027			
Mo	0.76	0.004	0.0038	0.0001	0.0063	0.0000	0.60	0.02	3
Ru	0.76	0.004	0.0079	0.0001	0.0015	0.0000	5.27	0.06	1
Re	0.76	0.002	0.0185	0.0008	0.0010	0.0000	18.50	0.80	4
BB-730 (21 h, 1250°C)									
Fe	77.86	0.737	0.8769	0.0012	0.6513	0.0014	1.35	0.00	0
Ni	9.92	0.089	0.1056	0.0009	0.0952	0.0007	1.11	0.02	2
S	9.92	0.164	0.0020	0.0001	0.2480	0.0020			
Mo	0.76	0.004	0.0016	0.0001	0.0032	0.0000	0.50	0.03	6
Ru	0.76	0.004	0.0072	0.0002	0.0017	0.0000	4.24	0.11	3
Re	0.76	0.002	0.0067	0.0006	0.0006	0.0000	11.17	1.00	9
BB-731 (20 h, 1150°C)									
Fe	79.08	0.744	0.8858	0.0007	0.6695	0.0018	1.32	0.01	1
Ni	10.08	0.090	0.0989	0.0000	0.0873	0.0004	1.13	0.01	1
S	10.08	0.164	0.0038	0.0002	0.2384	0.0018			
Re	0.77	0.002	0.0045	0.0002	0.0007	0.0001	6.43	1.40	22
BB-744 (27 h, 1250°C)									
Fe	79.08	0.744	0.9025	0.0025	0.6350	0.0018	1.42	0.01	1
Ni	10.08	0.090	0.0866	0.0002	0.0734	0.0004	1.18	0.01	1
S	10.08	0.164	0.0032	0.0022	0.2896	0.0020			
Re	0.77	0.002	0.0075	0.0001	0.0012	0.0000	6.25	0.08	1
BB-745 (43 h, 1300°C)									
Fe	77.86	0.737	0.9046	0.0010	0.6770	0.0015	1.34	0.00	0
Ni	9.92	0.089	0.0910	0.0009	0.0813	0.0003	1.12	0.01	1
S	9.92	0.164	0.0025	0.0004	0.2400	0.0015			
Mo	0.76	0.004	0.0002	0.0001	0.0014	0.0000	0.14	0.07	50
Ru	0.76	0.004	0.0012	0.0001	0.0003	0.0000	4.00	0.33	8
Re	0.76	0.002	0.0013	0.0001	0.0001	0.0000	13.00	1.00	8
BB-747 (52 h, 1100°C)									
Fe	77.86	0.737	0.9013	0.0009	0.5897	0.0010	1.53	0.00	0
Ni	9.92	0.089	0.0935	0.0011	0.0761	0.0005	1.23	0.02	2
S	9.92	0.164	0.0011	0.0001	0.3319	0.0009			
Mo	0.76	0.004	0.0005	0.0001	0.0020	0.0000	0.25	0.05	20
Ru	0.76	0.004	0.0024	0.0001	0.0001	0.0000	24.00	1.00	4
Re	0.76	0.002	0.0029	0.0004	0.0001	0.0000	29.00	4.00	14
BB-751 (72 h, 1100°C)									
Fe	75.18	0.729	0.8397	0.0064	0.6650	0.0047	1.26	0.02	2
Ni	9.22	0.085	0.0822	0.0009	0.0816	0.0006	1.01	0.02	2
S	9.22	0.156	0.0022	0.0001	0.2182	0.0031			
O	0	0.000	0.0112	0.0071	0.0144	0.0043			
Mo	2.13	0.012	0.0058	0.0002	0.0088	0.0001	0.66	0.03	5
Ru	2.13	0.011	0.0274	0.0003	0.0086	0.0002	3.17	0.12	4
Re	2.13	0.006	0.0315	0.0002	0.0033	0.0001	9.43	0.35	4
BB-753 (6 h, 1100°C)									
Fe	77.91	0.724	0.9045	0.0015	0.6660	0.0025	1.36	0.01	1
Ni	9.82	0.087	0.0854	0.0007	0.0746	0.0007	1.14	0.02	2
S	9.82	0.159	0.0030	0.0000	0.2309	0.0037			
O	0.61	0.020	0.0008	0.0013	0.0165	0.0029			
Mo	1.84	0.010	0.0064	0.0001	0.0119	0.0002	0.54	0.02	4

(Continued)

Table 1. (Continued)

Element	Starting comp.		Metal (at frac.)		Liquid (at frac.)		D	±	±
	wt %	At. Frac.	Avg	SD	Avg	$\sigma/\text{sqrt}(n)$	Metal/sulfide		%
BB-755 (6 h, 1000°C)									
Fe	77.05	0.715	0.9020	0.0023	0.5913	0.0027	1.53	0.01	1
Ni	9.84	0.087	0.0920	0.0010	0.0784	0.0006	1.17	0.03	3
S	9.84	0.159	0.0024	0.0000	0.2903	0.0009			
O	0.82	0.027	0.0008	0.0014	0.0228	0.0040			
Mo	2.46	0.013	0.0028	0.0004	0.0173	0.0002	0.16	0.03	19
BB-756 (6.5 h, 950°C)									
Fe	77.37	0.708	0.8770	0.0060	0.5364	0.0007	1.64	0.01	1
Ni	9.49	0.083	0.1148	0.0038	0.0961	0.0002	1.19	0.05	4
S	9.49	0.151	0.0012	0.0001	0.3483	0.0006			
O	1.46	0.047	0.0010	0.0016	0.0017	0.0012			
Mo	2.19	0.012	0.0060	0.0010	0.0176	0.0001	0.34	0.06	18
BB-757 (12 h, 950°C)									
Fe	77.34	0.720	0.8859	0.0018	0.5834	0.0022	1.52	0.01	1
Ni	10.16	0.090	0.1049	0.0012	0.0870	0.0005	1.21	0.02	2
S	9.38	0.152	0.0016	0.0000	0.3074	0.0013			
O	0.78	0.025	0.0000	0.0000	0.0038	0.0038			
Mo	2.34	0.013	0.0076	0.0006	0.0184	0.0003	0.41	0.04	10
BB-758 (22 h, 950°C)									
Fe	75	0.722	0.8595	0.0046	0.5802	0.0004	1.48	0.01	1
Ni	9.68	0.089	0.0726	0.0008	0.0712	0.0006	1.02	0.02	2
S	9.68	0.162	0.0011	0.0001	0.3348	0.0009			
O	0	0.000	0.0073	0.0053	0.0000	0.0000			
Mo	1.61	0.009	0.0052	0.0002	0.0120	0.0000	0.43	0.02	5
Ru	2.42	0.013	0.0246	0.0001	0.0016	0.0001	15.67	1.13	7
Re	1.61	0.005	0.0297	0.0004	0.0002	0.0000	141.43	1.9	1
BB-759 (28.5 h, 1000°C)									
Fe	76.35	0.733	0.8651	0.0014	0.5953	0.0024	1.45	0.01	1
Ni	9.46	0.086	0.0772	0.0007	0.0720	0.0003	1.07	0.02	2
S	9.46	0.158	0.0018	0.0001	0.3188	0.0023			
O	0	0.000	0.0000	0.0000	0.0004	0.0003			
Mo	1.35	0.008	0.0056	0.0002	0.0106	0.0001	0.53	0.02	4
Ru	2.03	0.011	0.0237	0.0001	0.0025	0.0001	9.48	0.44	5
Re	1.35	0.004	0.0267	0.0006	0.0005	0.0000	59.33	1.34	2
BB-760 (8.5 h, 1050°C)									
Fe	74.83	0.724	0.8535	0.0020	0.5781	0.0027	1.48	0.01	1
Ni	9.52	0.088	0.0817	0.0009	0.0775	0.0014	1.05	0.04	4
S	9.52	0.160	0.0014	0.0001	0.3227	0.0039			
O	0	0.000	0.0000	0.0000	0.0094	0.0025			
Mo	2.04	0.012	0.0064	0.0003	0.0092	0.0002	0.69	0.05	7
Ru	2.04	0.011	0.0268	0.0004	0.0026	0.0001	10.15	0.56	6
Re	2.04	0.006	0.0302	0.0007	0.0005	0.0000	62.92	1.46	2
BB-763 (19.5 h, 1000°C)									
Fe	76.86	0.726	0.8456	0.0077	0.5543	0.0036	1.53	0.02	1
Ni	9.92	0.089	0.0966	0.0018	0.0852	0.0005	1.13	0.03	3
S	9.92	0.163	0.0012	0.0001	0.3379	0.0014			
O	0	0.000	0.0066	0.0048	0.0133	0.0049			
Tc	2.48	0.013	0.0526	0.0092	0.0059	0.0001	8.95	1.72	19
Ti	0.83	0.009	0.0007	0.0002	0.0033	0.0001	0.21	0.06	29
BB-764 (21.5 h, 1100°C)									
Fe	76.52	0.724	0.8716	0.0029	0.5949	0.0036	1.47	0.01	1
Ni	9.85	0.089	0.0949	0.0007	0.0812	0.0008	1.17	0.02	2
S	9.85	0.162	0.0019	0.0001	0.3065	0.0024			
O	0	0.000	0.0012	0.0035	0.0062	0.0030			
Tc	3.03	0.016	0.0310	0.0003	0.0053	0.0002	5.83	0.28	5
Ti	0.76	0.008	0.0002	0.0000	0.0048	0.0001	0.04	0.01	25
BB-765 (8 h, 1200°C)									
Fe	75	0.716	0.8297	0.0041	0.5596	0.0024	1.48	0.02	1
Ni	9.68	0.088	0.1023	0.0021	0.0890	0.0006	1.15	0.03	3
S	9.68	0.161	0.0014	0.0002	0.3248	0.0029			
O	0	0.000	0.0014	0.0028	0.0054	0.0019			
Tc	4.84	0.026	0.0621	0.0010	0.0106	0.0002	5.84	0.21	4
Ti	0.81	0.009	0.0008	0.0008	0.0106	0.0003	0.08	0.07	88

(Continued)

Table 1. (Continued)

Element	Starting comp.		Metal (at frac.)		Liquid (at frac.)		D	±	±
	wt %	At. Frac.	Avg	SD	Avg	$\sigma/\text{sqrt}(n)$			
BB-766 (16 h, 1300°C)									
Fe	75.59	0.722	0.8579	0.0075	0.6648	0.0063	1.29	0.02	2
Ni	9.45	0.086	0.0904	0.0010	0.0842	0.0017	1.07	0.04	4
S	9.45	0.157	0.0020	0.0002	0.2213	0.0073			
O	0	0.000	0.0077	0.0087	0.0046	0.0063			
Tc	4.72	0.026	0.0420	0.0006	0.0163	0.0007	2.57	0.16	6
Ti	0.79	0.009	0.0001	0.0001	0.0088	0.0005	0.01	0.01	100
BB-767 (24 h, 950°C)									
Fe	75.37	0.719	0.8406	0.0043	0.5515	0.0019	1.52	0.02	1
Ni	9.7	0.088	0.0985	0.0006	0.0892	0.0006	1.10	0.02	2
S	9.7	0.161	0.0010	0.0003	0.3492	0.0011			
O	0	0.000	0.0054	0.0047	0.0042	0.0031			
Tc	4.48	0.024	0.0562	0.0016	0.0049	0.0001	11.47	0.50	4
Ti	0.75	0.008	0.0002	0.0002	0.0010	0.0001	0.20	0.23	115
LW-1 (8 h, 900°C, 1 bar)									
Fe	78.4	0.740	0.8863	0.0028	0.6198	0.0056	1.43	0.02	1
Ni	9.8	0.088	0.0941	0.0011	0.0696	0.001	1.35	0.04	3
S	9.8	0.161	0.0012	0.0001	0.2741	0.0052			
O	0	0.000	0.0094	0.0032	0.0307	0.0019			
Mo	2	0.011	0.0084	0.0003	0.0056	0.0001	1.5	0.08	5
Si	0	0.000	0.0006	0.0005	0.0003	0.0001	2	3.5	175

^a Experimental composition data, including starting bulk compositions, final metal and sulfide compositions, as well as calculated partition coefficients. Except for LW-1 in a sealed silica tube, all runs were performed at 60 kb in multianvil apparatus. Standard deviations of the mean are reported for the averages of the rastered quenched liquid compositions to approximate the uncertainty in the composition of the homogeneous liquid composition before quenching when phase separation added artificial variability to the analyses performed. The analyses of solid metal at the solid/liquid interface report standard deviations of replicate analyses as a measure of the compositional uncertainty in the solid metal composition.

significantly affect the Jones and Malvin (1990) partitioning systematics.

4. RESULTS

The partition coefficients are tabulated in Table 1 and plotted in Figures 4 to 6 versus the Jones-Malvin parameter, $-\ln(1 - 2\alpha X(S))$, where $\alpha = 1.09$ in the Fe-Ni-S system. Figures 4a and 4b compare $D(\text{Fe})$ and $D(\text{Ni})$ of the present work with previous studies representing different run conditions and experimental setups. The Fe data from other sources include 26 points at 1 bar from Jones and Malvin (1990), 11 points at 1 bar from Fleet et al. (1999), four points at 1 bar from Liu and Fleet (2000), and three points at 100 kb from Walker (2000). The Ni data from other sources include 43 points at 1 bar from Jones and Malvin (1990), 4 points at 1 bar from Fleet et al. (1999), 12 points at 60 kb from Wang (1993), and three points at 100 kb from Walker (2000). The figures generally demonstrate partitioning behavior consistent with Jones-Malvin systematics, i.e., linear behavior in these diagrams. The curvatures and anomalously low points in Figure 4 can be understood as deviations from strictly linear Jones and Malvin behavior through significant deviations from the ground rules. The matrix is not just for one system such as Fe-S across all these data sets. Changes in matrix lead to changes in α that are not accounted for in this summary figure which assumes a single generic value. That these results are compiled from a range of pressures suggests weak pressure dependence of metal-sulfide partitioning over a wide range of sulfur content. The departures of some of the 60 and 100 kbar data from the regression of the other pressures is thought to be more a function of the high Ir, Re, Os, and Pt

abundances in those experiments than of pressure (Wang, 1993; Walker, 2000). For example, the three 100 kbar points from Walker (2000) were for alloys with up to 60% Re + Os and ~30% Fe, a circumstance under which deviations from less bizarre compositions are easily imagined. We include our incidental Ti data in Figure 5. Ti displays a decreasingly chalcophile character as the sulfur content of the liquid increases and good Jones and Malvin systematics.

Our new Re and Ru partitioning data are plotted in Figure 6 and are consistent with previous studies. Both data sets demonstrate pressure independence over a wide range of sulfur concentration and a wide range in abundance of the tracer. Henry's Law and Jones and Malvin behavior are not violated. The Ru data from previous studies include two points at 1 bar from Liu and Fleet (2000). The Re data from previous studies includes seven points at 1 bar from Fleet et al. (1999) and three points at 100 kb from Walker (2000). Technetium is plotted in Figure 6 and is well behaved as a siderophile element in Jones and Malvin parameter space.

The data for Mo at 60 kbar in Table 1 and Figure 6 differ significantly from previous experiments at 1 bar. The previous data include four points from Liu and Fleet (2000), one point from Lodders and Palme (1991), and one point from Jones and Drake (1986). In the present study, all the high-pressure partitioning is in favor of the sulfide liquid, giving $D(\text{Mo}) < 1$. Furthermore the slope of the high-pressure $D(\text{Mo})$ variation in Figure 6 is zero or negative, suggesting chalcophile behavior. Previous studies (at 1 bar) have all given $D(\text{Mo}) > 1$ and variations with the Jones and Malvin parameter showing a positive slope. We were concerned that this discrepancy could

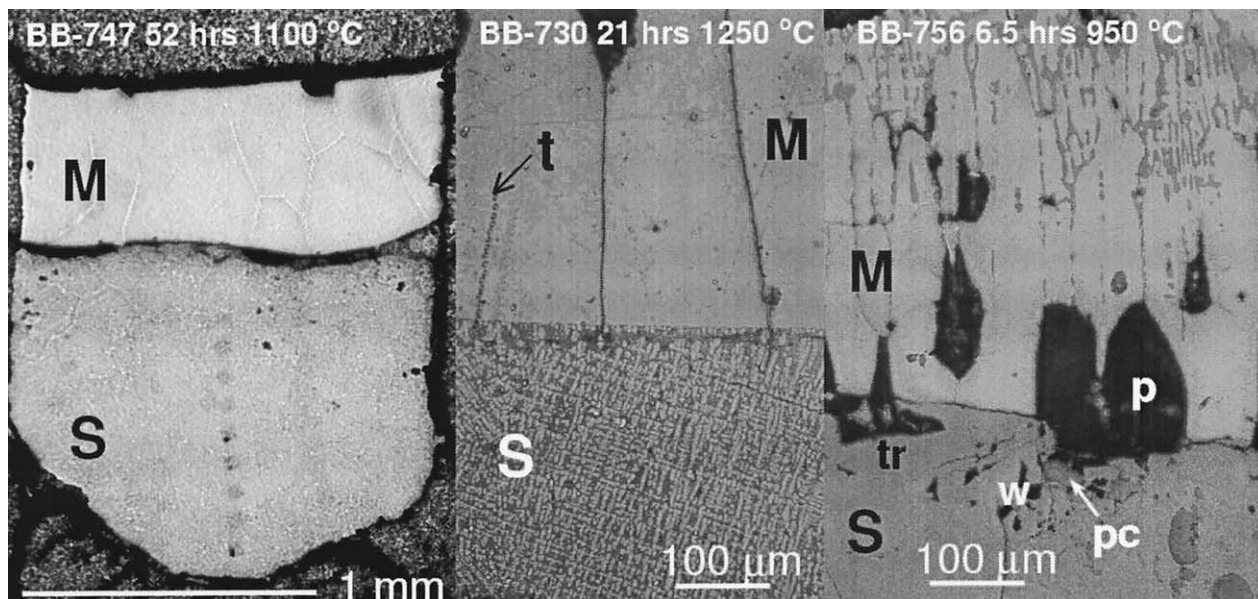


Fig. 1. Reflected light micrographs of three experiments after sectioning and polishing. "M" denotes the solid Fe-Ni metal alloy phase; "S" denotes the quenched sulfide liquid phase. A series of probe raster burns mark the traverse across the quenched sulfide liquid vertically near the middle of charge BB-747 in the first frame. The metal burn marks in the metal at the interface are too small to be seen at this scale. Burn marks in the metal phase are visible at higher magnification in BB-730 marked as traverse "t" in middle frame. Compositional information for this traverse is shown in Figure 3. The third frame for experiment BB-756 shows incompletely separated channels of sulfide liquid within the solid metal alloy at the top of the frame. The lower temperature and shorter time of BB-756 have not allowed the thermal migration process of the sulfide liquid globules to go to completion as it has in the previous two frames. The "tr" marks a large troilite crystal within the quenched sulfide liquid; "w" marks a wüstite-rich oxide next to dark crystals of a periclase-rich oxide marked "pc." The "p" tag denotes plucks of single crystals of metal removed during specimen preparation.

arise either because of the differences in analytical procedures used by the various studies to avoid the Mo $L\alpha$ overlap with the S $K\alpha$ X-ray emission line or because of the difference in experimental technique or pressure range of the different studies. Consequently, we performed an experiment with the evacuated silica tube procedures of Liu and Fleet (2000) using our

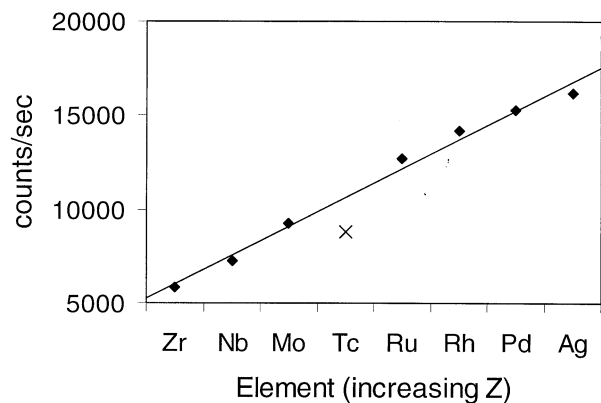


Fig. 2. Electron microprobe beam-generated X-ray intensity versus atomic number on a single spectrometer. Elements flanking Tc in the periodic table show a regular increase in beam intensity with atomic number. The concentration of Tc in our manufactured standard was initially estimated by dividing our measured Tc count rate from the standard by the interpolated count rate for pure Tc: (8800 counts per second)/(10700 counts per second) \times 100% \approx 82%.

Ni-bearing compositions. The cross in Figure 6 shows that our low-pressure experiment is in excellent agreement with the low-pressure experiments of Liu and Fleet (2000) so that analytical artifacts are not the cause of the unprecedented behavior seen in our 60 kbar data. Likewise Ni-free Liu and Fleet (2000)

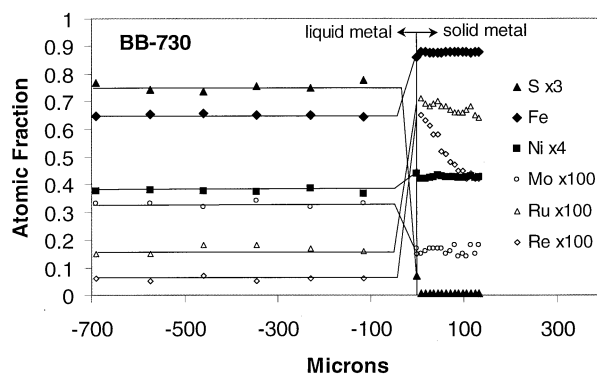
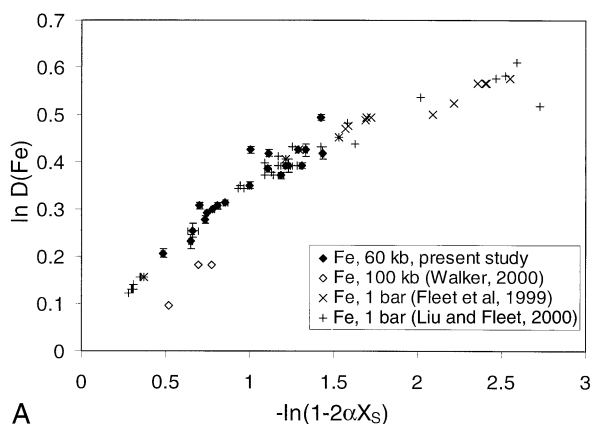
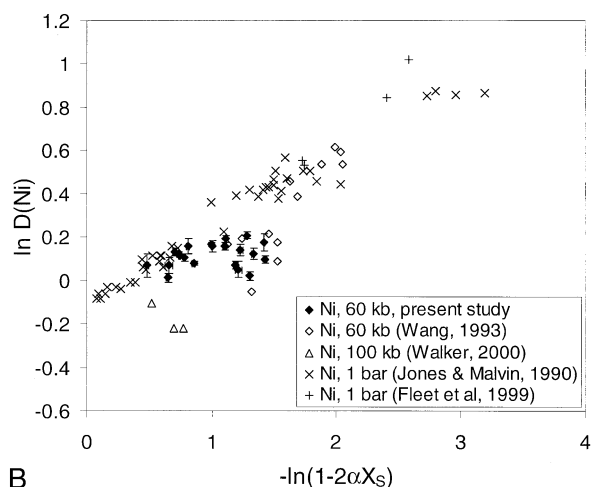


Fig. 3. Compositional information from traverse across experiment BB-730 shown in Figure 1, center panel. The traverse marked "t" in Figure 1, the closely spaced point array within the metal, appears on the right side of this figure at positive values on the position axis. Ru and especially Re show variation across the metal approaching the liquid/solid interface. The D values reported are calculated from the value for the solid metal at the interface and the average of the raster-mode analyses in the quenched liquid. The other elements in this experiment are fairly homogeneous in their respective phases. The interpretation of the residual gradients in Re and Ru follows that of Walker (2000).



A



B

Fig. 4. Partition coefficients versus sulfide concentration, plotted as $\ln D(x)$ vs. $-\ln(1 - 2\alpha X_S)$, the Jones and Malvin (1990) parameter. (a) and (b) contain our new Fe and Ni data compared with previous studies.

vs. Ni-bearing compositional issues are not at the root of the discrepancy because both our 60 kbar and silica tube experiments are Ni-bearing. A pressure effect on Mo partitioning appears to be the residual hypothesis capable of explaining the unusual behavior of Mo at 60 kbar which is divergent from all previous low-pressure experimental results and which is divergent from conventional positive-sloped Jones and Malvin systematics. Mo-sulfide speciation at high pressure rather than S-avoidance at low pressure would explain the results, but further observations are required for verification.

The apparent pressure effect may in part be due to a possible pressure-composition-mediated change from FCC to BCC Fe alloy structure (Brenan, personal communication). Both Ni and pressure enhance the FCC stability field. Mo stabilizes the BCC structure, which may have different partitioning behavior than the FCC structure. Especially at high pressure, 10% Ni might be expected to trump 2% Mo and give FCC Fe. However, the pressure effect we see might partially be Mo-introduction into the BCC structure at low pressure, even at high Ni content. Confirmation or refutation of this hypothesis would require more observations of the in situ Fe structure and partitioning behavior. In any case, this pressure effect exerts only a minor influence on our Mo partitioning conclusions relative to Tc

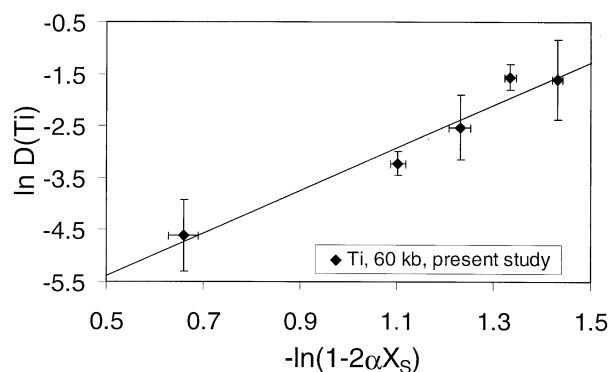


Fig. 5. Partitioning data for Ti as a function of the Jones and Malvin parameter which is a proxy for S concentration. Ti was present in the Tc experiments as a minor contaminant from the reduction procedure that converted oxidized Tc to metal using Ti foil and heat.

because $D(\text{Mo})$ approaches 1 at all S contents and pressures investigated whereas Tc is always fairly compatible in solid metal. Our calculations below for asteroidal cores make use only of the low pressure Mo data that have considerably less scatter than the high-pressure data, but the conclusions would not change if the high-pressure data had been used.

Some experiments yielded minor troilite, which generally crystallizes at the metal-sulfide interface. One experiment, BB-756 in the third frame of Figure 1, showed a troilite layer, euhedral wüstite, and Mo-rich phases in addition to metal and sulfide. The presence of other phases does not appear to affect the partitioning between metal and sulfide because systematic Jones and Malvin behavior of the Ds between metal and sulfide liquid is observed in both two-phase and polyphase charges. A few experiments captured channels of segregating sulfide within the metal, indicating the failure of the charge to reach a steady state, e.g., BB-756 in Figure 1. This pathology also appears to have little effect on the partitioning since the Ds calculated from the main mass of sulfide and the interface solid metal composition in such experiments are still consistent with the other data points.

5. DISCUSSION

Figure 6 compares the metal-sulfide partitioning of Tc, Mo, Ru, and Re. The parameters of the Jones-Malvin equation tabulated from linear regression of the data from Table 1 are provided in Table 2. The new data demonstrate that Tc partitioning behaves more similarly to Ru than Re, contrary to expectations based on the fact that Re and Tc occupy the same chemical period whereas Tc and Ru do not. Because Tc behaves very much like Ru (rather than Re), solid metal-liquid metal fractionation would likely lead to $<2\times$ changes in Tc/Ru, relative to the initial solar system average, except for metal produced by $>90\%$ fractional crystallization (Fig. 7a). This conclusion is based on modelling crystallization of a sizable asteroidal core with X_S ranging from 3.5 atom% (20 mg/g) to 30 atom% (198 mg/g). Such changes in S are consistent with 0 to 90% fractional crystallization of the group IIIAB iron meteorites that are believed to sample an asteroidal core (Wasson, 1999). Thus, detectable anomalies in Tc-induced ^{98}Ru and

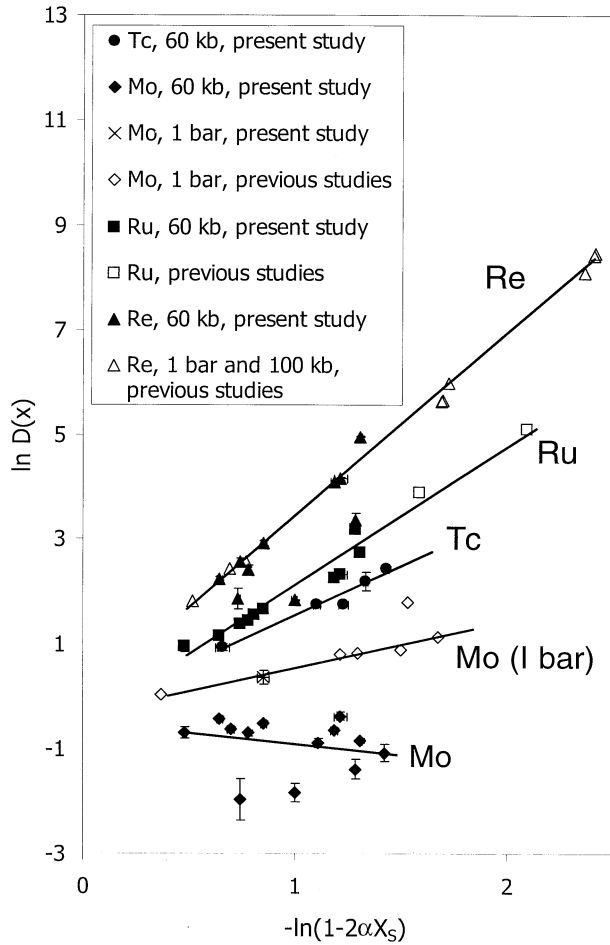


Fig. 6. Tc, Mo, Ru, and Re data versus the Jones and Malvin parameter compared with previous studies. Mo: Jones and Drake (1986), Lodders and Palme (1991), Liu and Fleet (2000). Ru: Fleet et al. (1999). Re: Fleet et al. (1999), Walker (2000). Tc behaves more like Ru than Re or Mo. The partitioning of Mo appears to be pressure-dependent.

^{99}Ru should not be expected for even very rapidly segregated and crystallized asteroidal cores. Using the Tc production assumptions of Becker and Walker (2003b), and fractionation within 2 Ma of Tc injection, the Tc/Ru of a metallic core would have to increase by a factor of approximately 6 relative to chondrites to generate a resolvable (positive) ^{98}Ru anomaly in iron crystallized from highly evolved liquids. This conclusion

Table 2. Parameters of the Jones-Malvin equation tabulated from fitting data in Table 1.

Jones-Malvin parameters for use in	$\ln(D) = \beta \ln(1 - 2\alpha X(S)) + C$	
	$-\beta$	C
$\alpha = 1.09$		
Re	3.40	-0.276
Ru	2.37	-0.341
Tc	1.85	-0.307
Mo 1bar	1.05	-0.427
Mo 60 kbar	-0.22	-0.707

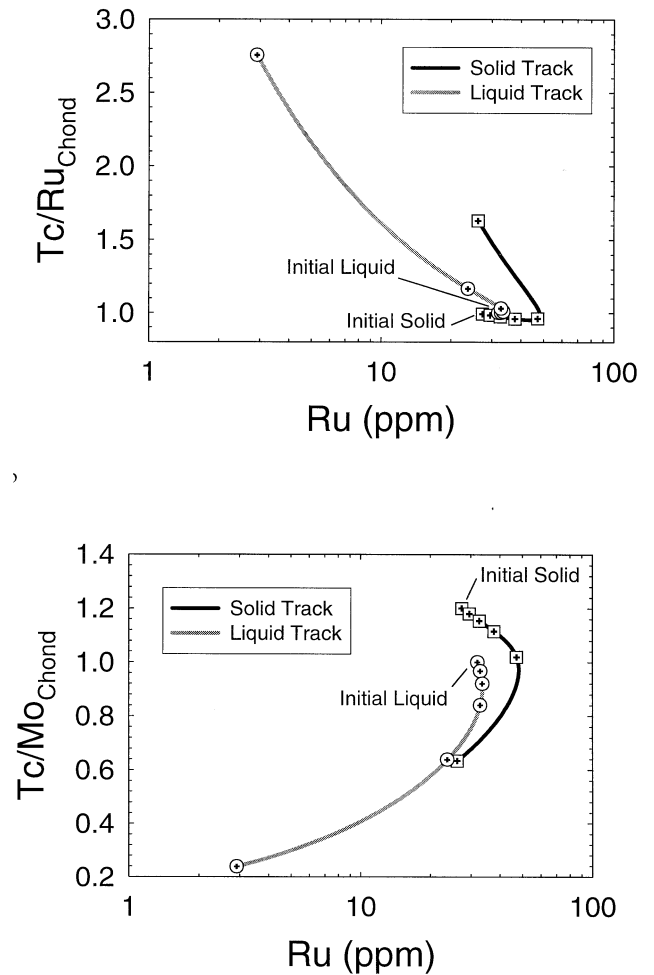


Fig. 7. (a) Ruthenium (ppm) versus Tc/Ru for 0–90% fractional crystallization of metal. The Tc/Ru is normalized to a hypothetical chondritic ratio. Calculations were made using D_{Tc} ranging from 0.85 ($S = 3.5$ atom%) to 5.3 ($S = 30$ atom%) and D_{Ru} ranging from 0.86 ($S = 3.5$ atom%) to 9.0 ($S = 30$ atom%). The starting liquid concentration for Ru is 32 ppm. Open squares and circles with crosses represent 0, 20, 40, 60, 80 and 90% fractional crystallization of the solid and liquid tracks, respectively. (b) Ruthenium (ppm) versus Tc/Mo for 0 to 90% fractional crystallization of metal. The Tc/Mo is normalized to a hypothetical chondritic ratio. Calculations were made using D_{Tc} as above, and D_{Mo} ranging from 0.71 ($S = 3.5$ atom%) to 2.0 ($S = 30$ atom%). Again, the starting liquid concentration for Ru is 32 ppm. Open squares and circles with crosses represent 0, 20, 40, 60, 80 and 90% fractional crystallization of the solid and liquid tracks, respectively.

is consistent with a recent study (Becker and Walker, 2003b), which found no ^{98}Ru or ^{99}Ru anomalies in iron meteorites. The conclusion, however, does not apply to materials that may result from other types of fractionation processes, such as core–mantle segregation.

The Tc–Mo system has deficiencies that are similar to those for the Tc–Ru system for constraining the time scales of asteroidal core crystallization. Although $D(\text{Tc})/D(\text{Mo})$ is always significantly greater than 1, 90% fractional crystallization leads to changes in Tc/Mo of only a factor of approximately $2\times$ in the IIIAB core crystallization model (Fig. 7b). Similar to Tc/Ru, the Tc/Mo of a rapidly fractionating metal system would

have to increase by more than approximately a factor of 8 to generate a resolvable (negative) ^{97}Mo anomaly in iron crystallized from highly evolved liquids. Recent studies of Mo isotopes in iron meteorites found no enrichments in ^{97}Mo above the 50 ppm level, consistent with these observations (Dauphas et al., 2002; Yin et al., 2002; Becker and Walker, 2003a).

Although not addressed by this study, we note that because Tc is highly siderophile and Mo only moderately siderophile, core–mantle segregation might be expected to lead to significantly subchondritic Tc/Mo ratios in silicate mantle relative to the solar system average. This is a mechanism that could lead to the generation of negative ^{97}Mo isotopic anomalies in some planetary mantles, provided that the initial abundance of ^{97}Tc in the solar system was sufficiently high.

Acknowledgments—We thank R. Anderson, G. Hamawy, and E. B. Watson for advice and assistance with the handling of ^{99}Tc in the laboratory. We thank J. Brenan, N. Chabot and anonymous reviewers for their helpful comments. This work was supported by the NSF CSEDI grants EAR0001963 (to DW) and EAR0001921 (to RJW). LDEO 6507 contribution.

Associate editor: B. Mysen

REFERENCES

- Becker H., Dalpe C., and Walker R. J. (2002) High precision Ru isotopic measurements by multi-collector ICP-MS. *Analyst* **127**, 775–780.
- Becker H. and Walker R. J. (2003a) Efficient mixing of the solar system from uniform Mo isotopic composition of meteorites. *Nature* **425**, 152–155.
- Becker H. and Walker R. J. (2003b) The ^{98}Tc - ^{98}Ru and ^{99}Tc - ^{99}Ru chronometers: New results on iron meteorites and chondrites. *Chem. Geol.* **196**, 43–56.
- Dauphas N., Marty B., and Reisberg L. (2002) Molybdenum evidence for inherited planetary scale isotope heterogeneity of the protosolar nebula. *Astrophys. J.* **565**, 640–644.
- Fleet M. E., Liu M., and Crocket J. H. (1999) Partitioning of trace amounts of highly siderophile elements in the Fe-Ni-S system and their fractionation in nature. *Geochim. Cosmochim. Acta* **63**, 2611–2622.
- Jana D. and Walker D. (1997) The influence of sulfur on partitioning of siderophile elements. *Geochim. Cosmochim. Acta* **61**, 5255–5277.
- Jones J. H. and Drake M. J. (1986) Geochemical constraints on core formation in the Earth. *Nature* **322**, 221–228.
- Jones J. H. and Malvin D. J. (1990) A nonmetal interaction model for the segregation of trace metals during solidification of Fe-Ni-S, Fe-Ni-P, and Fe-Ni-S-P alloys. *Metal. Trans. B* **21B**, 697–706.
- Jones J. H. and Walker D. (1991) Partitioning of siderophile elements in the Fe-Ni-S system: 1 bar to 80 kbar. *Earth Planet. Sci. Lett.* **105**, 127–133.
- Lee D. C. and Halliday A. N. (2002) Molybdenum isotopic anomalies in the accretion disk? (abstract 5135). 65th Ann. Meteoritical Society Meeting (CD-ROM).
- Liu M. and Fleet M. E. (2000) Partitioning of siderophile elements (W, Mo, As, Ag, Ge, Ga, and Sn) and Si in the Fe-S system and their fractionation in iron meteorites. *Geochim. Cosmochim. Acta* **65**, 671–682.
- Lodders K. and Palme H. (1991) On the chalcophile character of molybdenum: Determination of sulfide/silicate partition coefficients of Mo and W. *Earth Planet. Sci. Lett.* **103**, 311–324.
- Lu Q. and Masuda A. (1994a) The isotopic composition and atomic weight of molybdenum. *Int. J. Mass Spectr.* **130**, 65–72.
- Lu Q. and Masuda A. (2000) Variation of molybdenum isotopic composition in iron meteorites. In *Origin of the Elements in the Solar System: Implications of Post-1957 Observations* (ed. O. Manuel), pp. 385–399. Kluwer.
- Walker D. (1991) Lubrication, gasketing, and precision in multianvil experiments. *Am. Mineral.* **76**, 1092–1100.
- Walker D. (2000) Core participation in mantle geochemistry: Geochemical Society Ingerson Lecture, GSA Denver, October 1999. *Geochim. Cosmochim. Acta* **64**, 2897–2911.
- Walker D., Carpenter M. A., and Hitch C. M. (1990) Some simplifications to multianvil devices for high-pressure experiments. *Am. Mineral.* **75**, 1020–1028.
- Wang Y. (1993) Ir partitioning between metal-sulfide liquid and metal alloy. M.A. thesis. Columbia University.
- Wasson J. T. (1999) Trapped melt in IIIAB irons; solid/liquid elemental partitioning during the fractionation of the IIIAB magma. *Geochim. Cosmochim. Acta* **63**, 2875–2889.
- Yin Q. Z. (1995) Research for extinct ^{99}Tc and ^{98}Tc in the early Solar System. Ph.D. thesis. Johannes-Gutenberg Universität Mainz.
- Yin Q. Z. and Jacobsen S. B. (1998) The ^{97}Tc - ^{97}Mo chronometer and its implications for timing of terrestrial accretion and core formation. *Lunar Planet. Sci.* **29**, 1802.
- Yin Q. Z., Yamashita K., and Jacobsen S. B. (1999) Investigating the timescale of metal–silicate (core–mantle) differentiation using Hf-W and Tc-Mo extinct chronometers. In *Lunar Planet. Sci.* **30**, 2049.
- Yin Q. Z., Jacobsen S. B., and Yamashita K. (2002) Diverse supernova sources of pre-solar material inferred from molybdenum isotopes in meteorites. *Nature* **415**, 881–883.